Loss of MC1R signaling implicates TBX3 in pheomelanogenesis and melanoma predisposition

H. Matthew Berns[1,2], Dawn E. Watkins-Chow[1], Sizhu Lu[2], Pakavarin Louphrasitthiphol[2,3], Tongwu Zhang[4], Kevin M. Brown[4], Pedro Moura-Alves[2,5,6], Colin R. Goding[2], William J. Pavan[1,*]

[1]Genetic Disease Research Branch, National Human Genome Research Institute, National Institutes of Health, Bethesda, MD, 20892, USA.

[2]Ludwig Institute for Cancer Research, Nuffield Department of Clinical Medicine, University of Oxford, Headington, Oxford, OX3 7DQ, UK.

[3]Department of Gastrointestinal and Hepato-Biliary-Pancreatic Surgery, Faculty of Medicine, University of Tsukuba, Tsukuba, Japan.

[4]Division of Cancer Epidemiology and Genetics, National Cancer Institute, Bethesda, MD 20892, USA.

[5]i3S-Instituto de Investigação e Inovação em Saúde, Universidade do Porto, 4200-135 Porto, PT.

[6]IBMC-Instituto de Biologia Molecular e Celular, Universidade do Porto, 4200-135 Porto, PT.i3s

***Corresponding Author:** William J. Pavan

Email: bpavan@mail.nih.gov

Author Contributions: Contribution: W.J.P., D.E.W.-C, H.M.B, P.M.A., and C.R.G. designed the research study; H.M.B., D.E.W.-C, S.L., P.L., K.M.B., T.Z. acquired the data; H.M.B., D.E.W.-C, K.M.B., T.Z. analyzed data; H.M.B, D.E.W.-C, C.R.G., and W.J.P. wrote the manuscript; H.M.B., D.E.W.-C., S.L., P.L., C.R.G., P.M.A., and W.J.P. edited the manuscript; and all authors approved the final manuscript.

Financial Disclosure Statement:

This research was supported by the National Human Genome Research Institute (NHGRI) Intramural Research Program at the National Institutes of Health (NIH) (1ZIAHG000068-15), the Intramural Research Program of the National Cancer Institute (NCI) at the National Institutes of Health (NIH) (1ZIACP010201), and the Ludwig Institute for Cancer Research. H.M.B. is supported by an NHGRI Intramural Research Training Award, the NIH Oxford-Cambridge Scholars Program, and the NIH Medical Research Scholars Program, a public-private partnership supported jointly by the NIH and contributions to the Foundation for the NIH from the Doris Duke Charitable Foundation, Genentech, the American Association for Dental Research, and the Colgate-Palmolive Company. Additionally, P.M.A. would like to thank H2020-WIDESPREAD-2018-951921- ImmunoHUB for financial support. The funders had no role in study design, data collection and analysis, decision to publish, or preparation of the manuscript.

Competing Interest Statement: Authors have no competing interests to declare.

Keywords: melanoma; melanocytes; melanocortin 1 receptor (MC1R); TBX3; red hair color.

Data Availability: Original data created for the study are or will be available in a persistent repository upon publication. TBX3 ChIP is deposited in Gene Expression Omnibus (GEO) as GSE223256; Currently compiling pertinent information for submission of bulk and single-cell RNA-seq datasets to GEO.

Abstract

The human Red Hair Color (RHC) trait is caused by increased pheomelanin (red-yellow) and reduced eumelanin (black-brown) pigment in skin and hair due to diminished melanocortin 1 receptor (MC1R) function. In addition, individuals harboring the RHC trait are predisposed to melanoma development. While *MC1R* variants have been established as causative of RHC and are a well-defined risk factor for melanoma, it remains unclear mechanistically why decreased MC1R signaling alters pigmentation and increases melanoma susceptibility. Here, we use single-cell RNA-sequencing (scRNA-seq) of melanocytes isolated from RHC mouse models to reveal a Pheomelanin Gene Signature (PGS) comprising genes implicated in melanogenesis and oncogenic transformation. We show that TBX3, a well-known anti-senescence transcription factor implicated in melanoma progression, is part of the PGS and binds both E-box and T-box elements to regulate genes associated with melanogenesis and senescence bypass. Our results provide key insights into mechanisms by which MC1R signaling regulates pigmentation and how individuals with the RHC phenotype are predisposed to melanoma.

Introduction

Cancer predisposition is usually defined by inherited genetic mutations which increase an individual's risk of developing the disease. Identification of the genes and molecular pathways underlying predisposition is essential for both cancer treatment and prevention. Melanoma, the most lethal form of cutaneous cancer, arises from melanin-producing melanocytes and represents an excellent model to study cancer risk factors. Melanoma is an increasingly common skin cancer caused by high levels of sun exposure and subsequent damage by ultraviolet (UV) light. All stages of the disease are amenable to study and the genetic basis of disease initiation is well-defined. Specifically, cutaneous melanoma usually arises from acquisition of activated pro-oncogenes (e.g., BRAF, NRAS) combined with senescence bypass through inactivation of cell cycle regulators (e.g.,

71 CDKN2A/INK4A)[1–4]. However, in addition to genes falling into these two categories, additional
72 genetic loci have been implicated in melanoma predisposition. Understanding the molecular basis
73 for melanoma predisposition is a key issue which has the potential to inform melanoma prevention
74 strategies.

75 Red Hair Color (RHC) is a well-described melanoma predisposition phenotype. Individuals
76 with the RHC phenotype, possessing red hair, pale skin, freckles, and an inability to tan, show an
77 increased risk of developing melanoma compared to those with a non-RHC disposition[5–7]. The RHC
78 trait is mostly explained by coding variants of reduced function in the *melanocortin 1 receptor*
79 *(MC1R)* gene which encodes a G-protein-coupled receptor (GPCR) located on the cell surface of
80 melanocytes. MC1R signaling regulates pigment/melanin production[7–9]; therefore, diminished
81 MC1R function alters the ratio of cellular eumelanin and pheomelanin that largely determines skin,
82 hair, and eye color. Decreased MC1R signaling results in the loss of photoprotective eumelanin
83 synthesis and in turn allows for almost exclusive production of pheomelanin. High levels of
84 pheomelanin in RHC individuals exacerbate DNA damage through the amplification of free radicals
85 which is worsened when cells are exposed to UV[10,11], and pheomelanin itself can contribute to
86 melanomagenesis in the absence of UV radiation[11]. These observations may partly explain why
87 individuals with genetic RHC variants in *MC1R* exhibit an increased somatic mutational burden in
88 melanocytes[12].

89 Although the influence of *MC1R* RHC variants on melanin composition may play a role in
90 melanoma predisposition, *MC1R* mutation status may also have an impact on melanoma initiation
91 unrelated to its role in pigmentation. For example, individuals with *MC1R* variants fail to activate
92 PTEN upon UV exposure, resulting in increased PI3K/AKT signaling and oncogenic
93 transformation[13]. However, whether MC1R signaling plays additional roles in the prevention of
94 melanoma initiation remains unknown. In part, this may be because, by definition, a molecular
95 mechanism underlying melanoma predisposition must already be operating prior to the acquisition

96 of the ultimate trigger for melanoma initiation, such as acquiring activating BRAF or NRAS
97 mutations.

98 MC1R signaling shows high evolutionary conservation among mammals, thus murine
99 species provide an excellent model to explore this pathway. This includes mice with active MC1R
100 signaling (nonagouti; *a/a*), and suppressed MC1R signaling (recessive yellow, $Mc1r^{e/e}$, and lethal
101 yellow, A^y/a). Nonagouti mice have a dark coat color that results from a loss-of-function (LOF) allele
102 of the nonagouti gene (*a*), which encodes the mouse homolog of agouti signaling protein (ASIP).
103 In the absence of this important MC1R antagonist, nonagouti melanocytes predominantly
104 synthesize eumelanin. In contrast, recessive yellow ($Mc1r^{e/e}$) and lethal yellow (A^y/a) mice provide
105 two models for RHC, each with melanocytes that synthesize primarily pheomelanin due to distinct
106 molecular mechanisms which cause reduced MC1R signaling. Recessive yellow mice carry a LOF
107 allele in the MC1R receptor while the similar yellow coat color of lethal yellow mice is caused by
108 constitutive overexpression of the MC1R antagonist, agouti signaling protein[14–16].

109 Given the role of the RHC trait in melanoma risk, a better understanding of the genetic
110 regulatory network underlying aberrant MC1R signaling is needed. Previously, April et al[17] identified
111 several novel genes linked to pheomelanogenesis in mouse models using bulk RNA-sequencing.
112 Since this study used whole skin layers, of which melanocytes comprise only a small fraction of the
113 total cell population, gene expression from other cell types such as keratinocytes, basal cells, and
114 dendritic cells potentially masked the detection of melanocyte-intrinsic changes. Haltaufderhyde
115 and Oancea[18] performed bulk RNA-sequencing on human epidermal melanocytes to assess global
116 gene expression changes between light and dark colored cells. However, the genotypes were
117 unknown, and melanocytes were not exclusively producing one form of melanin over the other.
118 While these previous studies established an important foundation for our understanding of
119 pheomelanogenesis, additional, high-resolution genomic studies are needed to fully evaluate the

120 intricate molecular networks regulating eumelanogenesis, pheomelanogenesis, and melanoma
121 development.

122 To better understand the gene regulatory network associated with the RHC trait, we used
123 single-cell RNA-sequencing (scRNA-seq) to compare melanocytes with both active and
124 suppressed MC1R signaling. We defined a set of gene candidates, the Pheomelanin Gene
125 Signature (PGS), implicated in regulating pheomelanogenesis and melanomagenesis. We further
126 explored the chromatin occupancy of TBX3, a PGS- and melanoma-associated T-box family
127 member. Our results provide key insights into how RHC trait variants may increase melanoma risk
128 via altered regulation of PGS candidate genes downstream of MC1R.

129

130 Results

131 Single-cell RNA-sequencing of primary melanocytes identifies a 132 Pheomelanin Gene Signature (PGS)

133 To better understand global gene expression changes downstream of MC1R signaling, we used
134 single-cell RNA-sequencing (scRNA-seq) to define the transcriptomic profiles of primary mouse
135 melanocytes which predominantly synthesize either pheomelanin (lethal yellow, A^y; or recessive
136 yellow, $Mc1r^e$) or eumelanin (nonagouti, *a*). The dorsal skin was removed from post-natal day 3
137 (P3) animals along anatomically defined margins consisting of four incisions (Fig 1A): two
138 transverse cuts, with one between each axilla, and the other between the anterior pelvises, and
139 bilateral incisions at the midline from the axilla to the anterior pelvis. This tissue was then
140 enzymatically digested into a single-cell solution. Melanocytes comprise ~5% of cells within the
141 skin; therefore, after dissection and digestion of tissue, a fluorescent-activated cell sorting (FACS)
142 approach was used to enrich the pool of melanocytes for sequencing[19]. Positively selected cells
143 were defined as c-KIT$^+$ and CD45$^-$ (Fig 1A,B). To eliminate selection bias among potential
144 subpopulations of melanocytes that may vary in c-KIT levels, a lower intensity threshold for c-KIT
145 positivity was used, yielding a population enriched for melanocytes but expected to also contain

146 other cell types. Isolated cells were processed for library construction and RNA-sequencing via the
147 10x Genomics Chromium pipeline. After the implementation of quality control measures (see
148 Methods), sequencing data was obtained from a total of 11,058 cells from all samples. The
149 corresponding data underwent dimensional reduction via non-biased principal component (PCA)
150 and graph-based clustering analyses for graphical display by Uniform Manifold Approximation and
151 Projection (UMAP) (Fig 1C,D). We classified and labeled captured cell types by overlaying
152 published murine skin cell gene signatures[20] (Fig 1C,D; Table S1; Fig S1-S2). Cells classified as
153 melanocytes included 4 of the 16 graph-based clusters (GBC) identified in cells isolated from a
154 nonagouti and lethal yellow pair of samples, and 1 of 12 GBCs identified in cells isolated from a
155 nonagouti and recessive yellow pair of samples. Subsequently, for each of the 2 pairwise
156 experiments, all non-melanocyte cells were filtered out and only gene expression from the cells
157 classified as melanocytes were used for further analysis.

158 Because the mitotic stage has a significant and influential effect on gene expression, all
159 melanocytes outside the G_0/G_1 phase was removed using the same gene expression overlay
160 approach with previously published cell cycle marker genes[21,22] (Fig S3A, S3B). This defined the
161 non-cycling melanocytes that were used for differential gene expression analysis comparison.
162 Subsequent graph-based clustering analysis on the melanocyte population showed that both RHC
163 mouse models displayed a bifurcation between the pheomelanin melanocytes and the eumelanin
164 melanocytes captured in parallel, as displayed by UMAP (Fig 1C,D). Consistent with this, clustering
165 of melanocytes by genotype was unique to melanocytes and not observed in the other cell types,
166 suggesting that the effects of MC1R signaling loss are indeed restricted to melanocytes[23].

167 Using this melanocyte population, differentially expressed genes (DEGs) (ANOVA; FDR <
168 0.05 and fold-change (FC) ±2) were identified in pair-wise experiments to compare lethal yellow to
169 nonagouti melanocytes (Fig 1C) as well as recessive yellow to nonagouti melanocytes (Fig 1D).
170 The differential lists from each experiment were intersected to identify shared genes which have
171 consistent FC direction when comparing the nonagouti (*a/a*) melanocytes to the lethal yellow (A^y/a)
172 or recessive yellow ($Mc1r^{e/e}$) melanocytes. These comparisons resulted in a set of 216 genes which

173 we have identified as the Pheomelanin Gene Signature (PGS) (Table S2). We next asked to what
174 extent these genes are associated with pigmentation by querying the PGS against a compiled list
175 of genes annotated as causative for pigmentation phenotypes[24] to assess the degree of overlap.
176 Interestingly, only 5% of the PGS genes appeared in the previously annotated pigmentation gene
177 list (Table 1).

178 We next used PANTHER Gene Ontology (GO) and Ingenuity® Pathway Analysis (IPA) to
179 identify significantly over-represented processes and pathways in the PGS. GO analysis revealed
180 a prevalence of significant terms (FDR < 0.05) related to 'morphogenesis', 'melanin biosynthesis',
181 and 'neurogenesis' / 'neurotransmitter regulation' (Fig 2A). Terms related to 'melanin processes'
182 had equally high fold-enrichment; for example, 4 out of the 15 genes associated with 'melanin
183 biosynthetic process' are present in the PGS (*Tyrp1*, *Mc1r*, *Oca2*, and *Pmel*). IPA highlighted
184 canonical pathways related to 'Neuroinflammation, 'Synaptogenesis' and 'Neuron receptor
185 signaling' (Fig 2B). These terms are primarily driven by a host of receptors and ligands within the
186 gamma-aminobutyric acid (GABA), N-methyl-D-aspartate (NMDA)/Glutamate, Ephrin, and
187 Semaphorin families.

188

189 Predicted Transcriptional Regulators of the Pheomelanin Gene 190 Signature include TBX3

191 To better identify the gene regulatory network regulating pheomelanin synthesis, we examined
192 differentially expressed transcription factors, as well as predicted molecular upstream regulators of
193 gene regulatory networks. The PGS contains 22 annotated transcription and co-transcription
194 factors[25] (Fig 3A). Many of these have established relationships to melanocyte and pigment cell
195 biology, including neural crest development (*Hmga2*[26], *Id4*[27], *Mef2c*[28], *Tbx3*[29] and *Tfap2b*[30]),
196 melanocyte differentiation (*Mef2c*[31]), melanogenesis (*Id4*[32], *Irf4*[33], and *Tbx3*[34,35]), oxidative stress
197 protection (*Nr4a*[36]), and melanoma (*Hmga2*[37],*Irf4*[38], *Nfactc2*[39], *Nr4a*[40], *Tbx3*[41–45] and *Zeb1*[46–48]). Of
198 note, the *microphthalmia-associated transcription factor* (*Mitf*), a master melanocyte regulatory

199 transcription factor[49], was not identified as transcriptionally altered. Collectively, these data suggest
200 that pheomelanin synthesis is not simply a result of eumelanin synthesis inactivation, but rather
201 could involve multiple complex pathways downstream of MC1R signaling loss.

202 IPA was used to predict upstream regulators which may be driving expression of the PGS
203 (Fig 3B). The top 10 predicted regulators include three molecules -- SMAD4, GDF2, and SMAD1
204 -- that are all related to TGFβ/BMP signaling. Importantly, TGFβ signaling can regulate melanin
205 synthesis, with activation of the pathway resulting in hypopigmentation[50]. We reasoned that those
206 transcriptional targets downstream of TGFβ/BMP signaling merited further analysis. Among these
207 was *Tbx3*, a T-box family member activated by the TGFβ signaling pathway[51]. *Tbx3* showed
208 significantly increased expression in both the lethal yellow and recessive yellow samples (Fig 3A).
209 TBX3 has previously been implicated in melanoma invasion[44], but also has a key role as an anti-
210 senescence transcription factor[1–4,45,52]. Up-regulation of TBX3 and consequent suppression of
211 senescence in melanocytes lacking MC1R prior to acquisition of activating mutations in BRAF or
212 NRAS would therefore provide a potential mechanism by which redheads would exhibit a
213 predisposition to melanoma. In addition, TBX3 has previously been implicated in pigmentation, of
214 Dun horses for example[53], however, how TBX3 mediates these effects in unclear. Therefore, TBX3
215 was selected for further exploration with the goal of confirming TBX3 as a candidate transcription
216 factor for direct regulation of key anti-senescence and melanogenesis target genes downstream
217 from MC1R.

218

219 TBX3 binds at T-box and E-box motifs

220 To assess the functional targets of TBX3 in melanocytes, Chromatin immunoprecipitation
221 sequencing (ChIP-seq) was used to identify global targets of TBX3 binding. For this we used
222 doxycycline-inducible TBX3 tagged with an HA epitope previously used to produce high-quality
223 ChIP-seq datasets[54–56] (Fig S4A). In our studies, the level of induction of TBX3 by doxycycline was
224 adjusted to ensure physiological levels of TBX3-HA expression in the human melanoma cell line,
225 501mel (Fig S4B). We performed two replicate experiments and utilized MACS2 for peak calling

226 (q-value cutoff ≤ 0.01). To identify common peaks between the two replicates, a filter was applied
227 requiring an 80% overlap of coordinates between the 2 replicates, resulting in the identification of
228 20,449 common peaks (Fig S4C).

229 To determine the biological significance of these peaks, we used Genomic Regions
230 Enrichment Annotation Tool (GREAT)[57] to identify 10,000 peaks associated with 7,109 candidate
231 TBX3 gene targets (Methods; Table S3). We next assessed the binding distribution of these 10,000
232 peaks relative to gene transcriptional start sites (TSS). Promoter region binding within ±5kb of the
233 TSS comprised only 12.68% of peaks, and the vast majority were situated ±20kb from the TSS,
234 suggesting TBX3 binds distal enhancer elements (Fig 4A,B). GO enrichment for the 7,109
235 candidate TBX3 gene targets included multiple terms related to pigmentation/melanogenic
236 pathways, as well as multiple terms associated with EMT, of which TBX3 is a well-known regulator
237 (Fig 4C). Phenotype association analyses showed that pigmentation-related phenotypes were the
238 most abundant for both human and mouse with a particular emphasis on
239 hypopigmentation/abnormal melanocyte activity (Fig 4D).

240 We next used MEME-ChIP to assess motif enrichment within the TBX3 peaks. *De novo*
241 motif analysis revealed that the top 10 sequences (JASPAR CORE vertebrates non-redundant v2),
242 ranked by e-value, were not only associated with the expected T-box related elements, but also
243 with E-box related motifs (Fig 5A). Interestingly, the palindromic canonical E-box sequence
244 CACGTG is bound by basic-Helix-Loop-Helix (bHLH) and bHLHHzip transcription factors including
245 MITF and its related family member. This sequence shares a 3bp GTG with the well-described core
246 of the T-box element (AGGTGTGA) bound by T-box family members [55–57]. Furthermore, TBX3
247 represses *CDH1* at a CAGGTGT site which shares 5bp with the canonical E-box[44]. Interestingly, a
248 TBX3 peak does not appear at this site in our ChIP dataset; however, TBX3 and MITF share two
249 peaks within intron 2, and another peak 1.6kb upstream of the promoter region (Fig S4D).
250 Collectively, T-box and E-box motifs were found in the majority of TBX3-bound input sequences

251 (8,320/10,000; 83.20%) with the E-box motifs occurring more frequently than the T-box motifs
252 (69.17% vs 45.92%, respectively) (Fig 5B).

253 Importantly, as the E-box motif is the primary recognition sequence associated with MITF[49],
254 we wanted to interrogate the degree of shared genome-wide binding sites between TBX3 and
255 MITF. To assess for common occupancy of TBX3 and MITF we intersected our 20,449 TBX3 peaks
256 with 12,137 called peaks from a previously published human MITF ChIP dataset in 501mel cells[58].
257 This yielded 4,758 common peaks which were assessed with MEME-ChIP for motif enrichment.
258 The top 10 sequences (JASPAR CORE vertebrates non-redundant v2), ranked by e-value, were
259 all E-box related motifs (Fig 5C) centrally located within the TBX3 bound peaks (Fig 5D). The
260 frequency of TBX3 binding at centrally located E-box motifs also known to be occupied by MITF
261 suggests that TBX3 and MITF may compete for binding at a set of shared regulatory elements.

262 To query the set of TBX3 and MITF dual candidate target genes, we utilized the same
263 GREAT parameters as our TBX3 analysis to identify 7,095 MITF candidate target genes associated
264 with peaks from the MITF ChIP dataset[59] (Table S4). We then identified the mouse homologs for
265 both the TBX3 and MITF target gene sets to allow comparison to the PGS gene list derived from
266 *in vivo* mouse experiments (Table S5,S6). The intersection of TBX3 (6,499/7,109) and MITF
267 (6,661/7,094) gene target lists identified a shared set of 4,072 genes, representing 62.6% of the
268 TBX3 genome-wide target list (Fig 6A). Of these, 59 are found on the PGS (59/216; 27.3%),
269 suggesting that a portion of the PGS is directly regulated by both TBX3 and MITF (Fig 6B/Table
270 S7). Importantly, TBX3 and MITF shared binding sites at important pigmentation genes, with four
271 of these having well-described MITF regulatory elements *IRF4, MC1R, OCA2,* and *TYRP1*[59–62] (Fig
272 6C). Collectively, these data suggest that TBX3 can directly bind at E-box motifs associated with
273 PGS genes, thus regulating pheomelanogenesis via modulation of MITF-mediated gene regulation.
274

275 TBX3 functions as a transcriptional activator and repressor

276 Our bioinformatic analyses strongly suggest that TBX3 can bind near PGS genes, including
277 important genes related to melanogenesis. Traditionally, TBX3 has been shown to function as a

278 transcriptional repressor; however, it is known to include an activator domain[52,63]. In MC1R-
279 inhibited melanocytes, individual genes contained in the PGS exhibit either increased or decreased
280 expression relative to eumelanin-producing nonagouti melanocytes. Therefore, we wanted to
281 quantitatively analyze the extent to which TBX3 directly influences PGS expression levels. Bulk
282 RNA-sequencing in human melanoma cells was performed following the transient reduction of
283 TBX3, to determine (1) if the putative target genes were regulated by TBX3 and (2) if TBX3
284 repressed or activated these targets.

285 We performed transient knock-down of *TBX3* in 501mels for 24h, in triplicate, with two
286 distinct siRNAs (TBX3_13.6 and TBX3_13.8) and a non-coding control. At 24 hours we collected
287 lysates, harvested RNA, and then submitted samples for bulk RNA-seq. We then performed
288 differential analysis and identified significant DEGs (padj < 0.05) that were responsive to TBX3
289 depletion (Table S8). We next intersected DEGs from the two small interfering RNAs and removed
290 genes in which FC occurred in contradictory directions, resulting in 1,420 positive FC genes (+FC)
291 and 1,340 negative FC genes (-FC) (Fig 7A). To identify candidate genes regulated by TBX3, we
292 intersected this list with our TBX3 ChIP target genes, which identified a total of 1,091 targets (623
293 +FC, 468 -FC) that show both responsiveness to TBX3 depletion as well as TBX3 binding near
294 their respective genomic loci (Table S9).

295

296 TBX3 regulates PGS and cell cycle genes

297 We next performed Gene Set Enrichment Analysis (GSEA) on the candidate direct TBX3 targets
298 to identify significant (FDR < 0.05) KEGG terms associated with the +FC and -FC genes. Terms
299 for the +FC list include those related to TBX3's known role in melanoma, such as 'TGFb signaling
300 pathway', 'focal adhesion', and 'ECM receptor interaction' (Fig 7B). Importantly, 'melanogenesis'
301 was one of the most significant terms. Enriched terms for -FC genes include those consistent with
302 TBX3's pro-proliferative and anti-senescent functions, such as 'cell cycle', MAPK signaling
303 pathway', and 'p53 signaling pathway' (Fig 7B). Specifically, this includes cell cycle progression
304 genes *CDK1* and *CDK2* (Table S9). Lastly, we wanted to assess which PGS targets were

305 specifically bound and regulated in our *in vitro* system. We first converted the 1,091 +/- FC genes
306 bound and regulated by TBX3 to their known mouse homologs, yielding 1,041 genes. These were
307 intersected with the 98 genes comprising TBX3 targets of the PGS, of which 23 were present (Fig
308 7C). Collectively, these data suggest that TBX3 can regulate melanogenesis as both a
309 transcriptional activator and repressor of PGS genes.
310

311 # Discussion

312 Coding variants in *MC1R* are associated with the RHC trait. However, the gene regulatory networks
313 (GRNs) downstream of MC1R remain poorly understood. Through a high-resolution, single-cell
314 RNA-sequencing approach we have identified a Pheomelanin Gene Signature in melanocytes
315 comprising candidate genes which may regulate both pheomelanogenesis and melanomagenesis.
316 One such candidate is *Tbx3* which we show can bind and regulate PGS genes. Interestingly, we
317 have shown that the transcriptional regulatory activities of TBX3 include activation and repression
318 of candidate genes. Furthermore, this function is not restricted to DNA binding via the T-box motif,
319 rather it includes binding the canonical CACGTG E-box, which is the main recognition sequence of
320 the melanocyte master regulatory transcription factor MITF.
321 The vast majority of genes comprising the PGS have no previously established ties to
322 pigmentation phenotypes (205/216; 94.9%). A common approach to begin investigation of a novel
323 gene list involves identifying over-enriched gene families and pathways. One such PGS-enriched
324 family encompasses neurogenesis and neurotransmitter regulation and is primarily driven by
325 receptors and ligands within the gamma-aminobutyric acid (GABA), N-methyl-D-aspartate
326 (NMDA)/Glutamate, Ephrin, and Semaphorin families. Mature melanocytes show morphological
327 similarities with neurons in that they are highly dendritic, which enables contact with multiple
328 keratinocytes for melanin transfer. Furthermore, normal human melanocytes have GO enrichment
329 for 'neuron ensheathment and synapse'[22]. Interestingly, melanocytes that predominantly produce
330 pheomelanin in the presence of ASIP lack dendricity[64]. Likewise, inhibition of glutamate signaling

through NDMA receptors has been shown to inhibit melanocyte filipodia attachment to keratinocytes as well as reduce melanosome transfer efficacy[65]. A recent study has shown that GABA signaling between keratinocytes and melanoma cells occurs through neuronal like synapses, and further shows that this communication promotes melanoma initation[66]. Interestingly, in this context, keratinocytes showed increased GABA receptor expression while melanoma cells did not. Collectively, increased expression of these gene families may reflect both intrinsic and extrinsic signaling to promote melanocyte development, dendrite formation, and melanosome transfer abilities.

Previous work has shown that the benzodiazepine Diazepam, which works to increase the action of GABA, increases both melanogenesis and melanocyte dendricity[67]. Likewise, NMDA receptors appear to promote melanin synthesis and tyrosinase activity in the cuttlefish, *Sepia officinalis*[67,68]. In addition, glutamate receptor genes, especially *Grm1*, are expressed in human melanomas[69], and ectopic expression of *mGluR1* in melanocytes leads to oncogenic transformation and metastatic spread with 100% penetrance[69]. Ephrins play an essential role in regulating biological processes such as cell-cell attachment, cell shape, and motility[70]. Along with Semaphorins, they are expressed in neural crest cells (which give rise to melanocytes) and are of vital importance in regulating neural crest migration[71]. Genes within these families also show differential expression in melanocytes treated with ASIP, suggesting that this treatment results in dedifferentiation towards a neural crest-like state[72]. Our data further validate this idea and suggest that MC1R acts downstream of ASIP to effect these changes, as loss of MC1R in primary melanocytes drives similar gene expression changes.

Transcription factors play an essential role in the regulation of gene expression. The most well-characterized of these in melanocytes is *Mitf.* This gene encodes a master regulatory transcription factor implicit in melanocyte specificity, proliferation, survival, migration, differentiation, and melanogenesis, and whose expression has been reported to lie downstream from MC1R signaling[73,74]. *Mitf* does not exhibit differential expression in our study, nor do many of its known post-transcriptional/translational modifiers, such as MAPKs, *Gsk3b*, *p300*, and *Stat3,*

358 although changes in the activity of these signaling molecules may not be apparent in the gene
359 expression profile. Similarly, other well-characterized transcription factors in melanocyte biology,
360 including *Sox10*, *Pax3*, *Lef1*, and *Creb,* which can all regulate *Mitf,* also exhibit no differential
361 expression. This supports that the primary transcriptional changes driving activation of
362 pheomelanin, and repression of eumelanin, synthesis downstream of MC1R signaling are not
363 mediated through reduced *Mitf* transcription, but instead through transcriptional regulation of other
364 factors that modulate the DNA binding or post-transcriptional regulation of MITF.

365 One of the primary candidate genes we performed further analysis on is the T-box
366 transcription factor family member, *Tbx3*. This candidate stood out for the following reasons: (1) it
367 is activated by TGFβ/BMP signaling[51,63,75], (2) it has high fold-enrichment in melanocytes from both
368 pheomelanin-producing mouse genotypes (Fig 3A), (3) it is found across multiple terms from our
369 GO analysis, (4) it has known functional roles in developmental states of melanocytes[29,34,35] (5) it
370 regulates developmental processes across multiple tissue/cell types, including heart[76–78], lungs[79],
371 limbs[80,81], inner ear[82], and neural crest[29,76], and (6) is highly expressed in a multitude of cancers,
372 especially melanoma, where its primary roles appear to be in metastasis by activation of EMT, at
373 least in part through down-regulation of E-cadherin, as well as suppression of senescence[41,43–
374 45,83,84].

375 The differential expression of *Tbx3* in eumelanin- and pheomelanin-expressing
376 melanocytes, along with genome-wide binding of TBX3 to T- and E-box elements in melanoma
377 cells, suggested that TBX3 may directly regulate MITF targets downstream of MC1R signaling.
378 Through ChIP and bulk RNA-seq we've shown that TBX3 can bind and regulate genes within the
379 PGS. Although TBX3 is often viewed as a transcriptional repressor, it has been shown to activate
380 gene expression of putative target genes[52]. Likewise, our data strongly suggests that TBX3 can
381 both activate or repress target genes. These targets include genes with known associations to
382 pigmentation phenotypes. An intriguing example of TBX3-mediated activation is *Slc7a11*. This
383 gene encodes the cystine/glutamate exchanger (xCT) which imports cystine into the cell where it
384 is reduced into two molecules of cysteine, a necessary component for pheomelanin synthesis[85,86].

385 The increased pool of cysteine provides an environment that is favorable for pheomelanin
386 synthesis. Increased expression of *Slc7a11* by TBX3 suggests an active process downstream of
387 MC1R to favor pheomelanin synthesis, distinct from the repression of eumelanin synthesis. The
388 importance of cysteine goes beyond pheomelanin synthesis, as it is an essential factor of the
389 glutathione system and oxidative stress regulation as well as ferroptosis inhibiton[86,87]. Following
390 *TBX3* knockdown we observed a significant reduction of *SLC7A11* expression, with associated
391 enrichment of pathways associated with 'glutathione metabolism' and 'apoptosis'. Given the
392 cytotoxicity of pheomelanin, regulation of cysteine levels within melanocytes is critical and presents
393 a paradox where cysteine is essential for regulating oxidative stress; however, too much can
394 exacerbate cell stress through pheomelanin accumulation.

395 TBX3 is implicated in senescence by-pass partly through its ability to repress cell cycle
396 checkpoint genes such as CDKN2B[52]. Our *TBX3* knockdown data support this, with *CDKN2B*
397 showing significantly increased expression. Furthermore, our data also support a role for TBX3 in
398 senescence by-pass through activation of cell cycle progression genes, where the loss of *TBX3*
399 yields decreased expression of *CDK1* and *CDK2* (Table S9). Willmer et al[88] have shown that TBX3
400 is important in S-phase transition in part due to post-translational phosphorylation via CDK2[88]. More
401 recent work from this group suggests a more complex relationship, whereby TBX3 itself promotes
402 *CDK2* expression[89]. Our data further support this model and suggest a further way in which TBX3
403 can contribute to oncogenic transformation by facilitating senescence bypass. These observations
404 may pave the way in explaining why redheads with diminished MC1R function may be predisposed
405 to melanoma.

406 The T-box family members comprise five sub-groups, with TBX3 as a member of the TBX2
407 sub-group. TBX2 and TBX3 share 95% homology within the DNA binding domain[63]. TBX2, which
408 canonically binds the T-box, can also bind the E-box motif, and functions as both an activator and
409 repressor[56]. Our data support the idea that TBX3 also binds to, and regulates gene expression, via
410 the E-box motif. However, unlike TBX2, the type of motif bound does not seem to influence its
411 action (Fig S5A). E-box site recognition of TBX3 can possibly be explained with protein structural

412 studies. As mentioned previously, the canonical E-box and T-box elements share a 3bp (GTG)
413 region. This corresponds to base pairs 3-5 of the T-box (AGGTGTGA). Consequently, this 3bp core
414 significantly affects TBX3's ability to bind DNA, whereas the flanking base pairs are deemed less
415 crucial[90]. As a monomer, TBX3 can also bind to either the major or minor groove[90]. Therefore, while
416 bound in the minor grove, it is possible that TBX3 may interact with other transcription factors bound
417 in the major grove, including MITF. The degree to which TBX3 modulates gene expression is most
418 likely dependent on several factors, including, cell type, differentiation state, co-factor availability,
419 chromatin accessibility, and biological state (e.g., methylated, acetylated). Variation across these
420 factors could explain why more putative genes targets regulated by TBX3 in human melanoma
421 cells *in vitro* are not represented in the *in vivo* healthy murine melanocyte PGS.

422 In this study, we aimed to profile the transcriptome in melanocytes with aberrant MC1R
423 signaling. To this end we have defined a set of genes (PGS) that merit further investigation towards
424 better understanding the complex GRNs downstream of MC1R signaling. This includes the
425 melanoma-associated transcription factor, *Tbx3*. Furthermore, we believe the Pheomelanin Gene
426 Signature provides important candidate genes that merit further follow-up regarding the regulation
427 of melanocyte development, melanogenesis, and melanomagenesis.

428

429 Materials and Methods

430 Single-Cell RNA-Sequencing and Differential Expression 431 Analysis

432 FACS-isolated melanocytes were captured in a solution of 1xPBS + 0.04% FBS. Cell viability and
433 concentration were analyzed using a Luna-FX7 cell counter (Logos Biosystems). Gel Bead-in-
434 Emulsions were prepared by loading 5,000 cells/sample onto a Chromium Chip G (10x Genomics
435 #1000127) and run using the Chromium controller (10x Genomics #1000204). cDNA libraries were
436 generated with Chromium Single Cell 3' GEM, Library and Gel Bead Kit V3.1 (10x Genomics
437 #1000128). Samples were indexed and pairs for each experiment were pooled for sequencing

438 using the NextSeq 500/550 Hi Output KT v2.5 (Illumina #20024907) on an Illumina NextSeq550.
439 Barcoded reads were aligned to the mm39 genome using STAR aligner. Downstream processing
440 of the data was performed with Partek Flow™ Genomic Analysis Software.
441 Single cell QA/QC included steps to filter out cells which did not meet the following parameters
442 defined in the two pairwise experiments (lethal yellow / recessive yellow) as: barcode count 600-
443 32,000/3,000-45,000, number of genes detected 500-6000/500-7000, and % ribosomal counts 12-
444 43%/12-39%. Of the 31,017 annotated murine genes, 16,793 (54.14%)/20,060 (64.7%) passed an
445 exclusion cutoff where genes were excluded if they had zero counts in at least 99.9% of the cells.
446 The remaining read counts were normalized using a $\log_2$-based method on Counts Per Million
447 (CPM). Normalized counts underwent dimensional reduction via a Principal Components Analysis
448 (PCA) on the first 100 principal components and unsupervised, non-biased, Graph-based
449 clustering through a Louvain algorithm on the first 20 principal components. Graph-based clusters
450 underwent further dimensional reduction for visualization on a Uniform Manifold Approximation and
451 Projection diagram. Postnatal mouse skin cell types including dermal fibroblasts, dermal papilla,
452 transit amplifying cells, matrix cells, and epidermal cells were identified by utilizing published
453 signature gene lists[20]. The most highly expressed genes (top 10%) from the signature gene lists
454 were overlayed on the UMAP and the graph-based clusters which coincided with expression
455 overlay were assigned to each cell type. All non-melanocyte cell types were subsequently filtered
456 out, leaving only clusters classified as melanocytes for downstream analysis. The melanocyte only
457 population underwent a further iteration of PCA, graph-based clustering, and UMAP display. To
458 eliminate the variable of cellular heterogeneity as influenced by the mitotic state, we selected for
459 cells within the G_0 phase using a gene expression overlay established by Hsiao et al[21]. The
460 melanocytes within the G_0 phase underwent a further iteration of PCA, graph-based clustering, and
461 UMAP analysis. Differential gene expression lists of melanocytes were generated using the Partek
462 ANOVA differential expression analysis. Genes considered statistically significant had a False-
463 discovery rate of <0.05 and a fold-change of ±2.
464

465 ## Gene ontology and pathway analysis

466 Genes comprising the Pheomelanin Gene Signature were uploaded to the Gene Ontology
467 Resource for GO Enrichment Analysis via PANTHER for Overrepresentation Tests (GO Ontology
468 database DOI:10.5281/zenodo.6399963; Released 2022-03-22). The PGS was run against a
469 reference list comprising all *Mus musculus* genes in the database. Fisher's Exact test was
470 performed with a False Discovery Rate correction for GO Biological Process Complete, GO Cell
471 Component Complete, and GO Molecular Function Complete with significant results being those
472 with an FDR < 0.05. To identify predicted upstream regulators, we utilized QIAGEN's Ingenuity®
473 Pathway Analysis (73620684 (Release Date: 2022-03-12). Testing was done via Expression Core
474 Analysis on the observed experimental fold change of the PGS for both pairwise experiments.
475

476 ## Gene Set Enrichment Analysis

477 Gene lists comprising the significant DE +FC and -FC genes regulated by TBX3 were uploaded to
478 the Molecular Signatures Database (MSigDB) for gene set enrichment analysis utilizing the Kyoto
479 Encyclopedia of Genes and Genomes (KEGG). For the +FC list, the top 500 genes by fold-change
480 for TBX3_13.8 were used as the maximum input value is 500 genes. Each list was tested
481 independently with significant terms being those with an FDR q-value < 0.05.
482

483 ## TBX3 ChIP Analysis

484 Prior to mapping to the human reference genome (hg38) with Bowtie2 (v.2.3.5)[91], quality of the raw
485 sequencing data was evaluated using FastQC (v.0.11.7), with adapter contamination removed
486 using CutAdapt (v.2.8). Peak calling was performed using MACS2 (v.2.1.2)[92] with a 0.01 q-value
487 threshold. Bowtie2-generated SAM files were compressed to BAM files, indexed using SAMtools
488 (v.1.9), and sequentially converted to bigWig files using USCStools (v.373). The BED files of both
489 replicates were intersected using the UCSC Table Browser to pull out common peaks from replicate
490 2 (40,974) that had ≥80% overlap with replicate 1 (32,479), which yielded a group of 20,449

491 common peaks. For simplicity of downstream analysis, the 20,449 peak coordinates used were
492 derived from the BED position parameters of replicate 1.
493 The Genomic Regions Enrichment of Annotations Tool (GREAT v4.0.4)[57] was used to analyze the
494 functional significance of cis-regulatory regions of the TBX3 bound ChIP peaks. Each annotated
495 gene was assigned a basal regulatory domain of 5kb upstream, and 1kb downstream, of the
496 transcriptional start site. The regulatory domain of that gene was then extended in both directions
497 to the nearest gene's basal domain but with no more than a 100kb extension in one direction[57].
498 Discovery of enriched binding motifs was done using the MEME-ChIP[93] DNA binding motif analysis
499 tool. 250bps were added up and downstream of the chromosomal coordinates corresponding to
500 the absolute summit of all overlapping peaks. A FASTA file was generated using the usegalaxy.org
501 bedtools application 'GetFastaBed'[94]. This was run against the default settings in MEME-ChIP,
502 except for maximum width for 'What width motifs should MEME and STREME find?' which was
503 increased to 20 bases. Peak distributions were obtained from GREAT and ChIPseeker[95], via
504 usegalaxy.org. The histogram was produced by GREAT, while the venn diagram was created with
505 ChIPseeker.
506

507 Bulk RNAseq of *in vitro* 501mel Human Melanoma Cells

508 501mel cells (140,000/well) were plated in a 12-well plate (1.2mL/well). dsiRNAs (NC1, TBX3 13.6,
509 TBX 13.8; Integrated DNA Technologies) were diluted in 300uL of Opti-MEM (final concertation of
510 20nM). Lipofectamine RNAiMAX (6uL/100uL; Invitrogen 13778075) was then diluted in 300uL of
511 Opti-MEM. Diluted dsiRNA and Lipofectamine were mixed and set to incubate at RT for 5 mins.
512 200ul of dsiRNA-Lipofectamine mix was added to each well. At 24h, cells were lysed for RNA
513 collection via (Zymo Research R2053). RNA purity was assessed via tapestation with all samples
514 having a RIN purity of ≥ 9.0. RNA samples were submitted to Omega Bioservices (Norcross, GA,
515 USA) for bulk RNAseq. RNA purity was again assessed via an Agilent tapestation with all samples
516 having a RIN ≥ 9.0. Library construction was completed using NEBNext® Ultra™ II Directional RNA
517 Library Prep Kit for Illumina®. Samples were sequenced using NovaSeq 6000 (Illumina) PE150

518 with a ~40M (20M in each direction) read throughput for each sample. Phred Mean Quality scores
519 for all samples was ≥ 38.86. Data were analyzed by ROSALIND® (https://rosalind.bio/), with a
520 HyperScale architecture developed by ROSALIND, Inc. (San Diego, CA).
521

522 Figure Construction

523 Figures were assembled and created with BioRender.com. UMAPs were generated with Partek
524 Flow. Venn diagrams were produced using DeepVenn. Binding distribution, Fig 3A, was modified
525 from original GREAT output, while Fig 3B was modified from the ChIP seeker output from
526 usegalaxy.org. Motif distribution for Fig 5D is modified from the MEME CentriMo tool.
527
528

529 Acknowledgments

530 We are grateful to Dr. Jonathan Zippin for providing the C57BL/6J-Mc1r^{e}/J mice and helpful
531 scientific discussion. We further extend thanks to the NHGRI Microarray (Dr. Abdel G. Elkahloun
532 and Bayu Sisay) and Flow Cytometry (Stacie Anderson and Martha Kirby) cores. Lastly, we greatly
533 appreciate the help of Dr. Laura Baxter in providing helpful editing and feedback.

534 # References

535 1.) Ha, L., Merlino, G. & Sviderskaya, E. V. Melanomagenesis: Overcoming the barrier of
536 melanocyte senescence. *Cell Cycle* **7**, 1944–1948 (2008).
537 2.) Bennett, D. C. & Medrano, E. E. Molecular Regulation of Melanocyte Senescence. *Pigm*
538 *Cell Res* **15**, 242–250 (2002).
539 3.) Vredeveld, L. C. W. *et al.* Abrogation of BRAFV600E-induced senescence by PI3K
540 pathway activation contributes to melanomagenesis. *Gene Dev* **26**, 1055–1069 (2012).
541 4.) Wagstaff, W. *et al.* Melanoma --- Molecular genetics, metastasis, targeted therapies,
542 immunotherapies, and therapeutic resistance. *Genes Dis* **9**, 1608–1623 (2022).
543 5.) Rhodes, A. R., Weinstock, M. A., Fitzpatrick, T. B., Mihm, M. C. & Sober, A. J. Risk
544 Factors for Cutaneous Melanoma: A Practical Method of Recognizing Predisposed
545 Individuals. *Jama* **258**, 3146–3154 (1987).
546 6.) Rayner, J. E. *et al.* Phenotypic and genotypic analysis of amelanotic and hypomelanotic
547 melanoma patients. *J Eur Acad Dermatol* **33**, 1076–1083 (2019).
548 7.) Schiöth, H. B. *et al.* Loss of Function Mutations of the Human Melanocortin 1 Receptor
549 Are Common and Are Associated with Red Hair. *Biochem Bioph Res Co* **260**, 488–491
550 (1999).
551 8.) Pavan, W. J. & Sturm, R. A. The Genetics of Human Skin and Hair Pigmentation. *Annu*
552 *Rev Genom Hum G* **20**, 1–32 (2019).
553 9.) Mort, R. L., Jackson, I. J. & Patton, E. E. The melanocyte lineage in development and
554 disease. *Development* **142**, 620–632 (2015).
555 10.) Napolitano, A., Panzella, L., Monfrecola, G. & d'Ischia, M. Pheomelanin-induced
556 oxidative stress: bright and dark chemistry bridging red hair phenotype and melanoma.
557 *Pigm Cell Melanoma R* **27**, 721–733 (2014).
558 11.) Mitra, D. *et al.* An ultraviolet-radiation-independent pathway to melanoma carcinogenesis
559 in the red hair/fair skin background. *Nature* **491**, 449–453 (2012).

560 12.) Robles-Espinoza, C. D. *et al.* Germline MC1R status influences somatic mutation burden
561 in melanoma. *Nat Commun* **7**, 12064 (2016).
562 13.) Cao, J. *et al.* MC1R Is a Potent Regulator of PTEN after UV Exposure in Melanocytes.
563 *Mol Cell* **51**, 409–422 (2013).
564 14.) HAUSCHKA, T. S., JACOBS, B. B. & HOLDRIDGE, B. A. Recessive Yellow and its
565 Interaction With Belted in the Mouse. *J Hered* **59**, 339–341 (1968).
566 15.) Michaud, E. J., Bultman, S. J., Stubbs, L. J. & Woychik, R. P. The embryonic lethality of
567 homozygous lethal yellow mice (Ay/Ay) is associated with the disruption of a novel RNA-
568 binding protein. *Gene Dev* **7**, 1203–1213 (1993).
569 16.) Michaud, E. J. *et al.* A molecular model for the genetic and phenotypic characteristics of
570 the mouse lethal yellow (Ay) mutation. *Proc National Acad Sci* **91**, 2562–2566 (1994).
571 17.) April, C. S. & Barsh, G. S. Skin layer-specific transcriptional profiles in normal and
572 recessive yellow (Mc1re/Mc1re) mice. *Pigm Cell Res* **19**, 194–205 (2006).
573 18.) Haltaufderhyde, K. D. & Oancea, E. Genome-wide transcriptome analysis of human
574 epidermal melanocytes. *Genomics* **104**, 482–489 (2014).
575 19.) Harris, M. L. *et al.* A direct link between MITF, innate immunity, and hair graying. *Plos*
576 *Biol* **16**, e2003648 (2018).
577 20.) Rezza, A. *et al.* Signaling Networks among Stem Cell Precursors, Transit-Amplifying
578 Progenitors, and their Niche in Developing Hair Follicles. *Cell Reports* **14**, 3001–3018
579 (2016).
580 21.) Hsiao, C. J. *et al.* Characterizing and inferring quantitative cell cycle phase in single-cell
581 RNA-seq data analysis. *Genome Res* **30**, 611–621 (2020).
582 22.) Belote, R. L. *et al.* Human melanocyte development and melanoma dedifferentiation at
583 single-cell resolution. *Nat Cell Biol* 1–13 (2021) doi:10.1038/s41556-021-00740-8.
584 23.) Guida, S., Guida, G. & Goding, C. R. MC1R Functions, Expression, and Implications for
585 Targeted Therapy. *J Invest Dermatol* (2021) doi:10.1016/j.jid.2021.06.018.

586 24.) Baxter, L. L., Watkins-Chow, D. E., Pavan, W. J. & Loftus, S. K. A curated gene list for
587 expanding the horizons of pigmentation biology. *Pigm Cell Melanoma R* **32**, 348–358
588 (2019).
589 25.) Hu, H. *et al.* AnimalTFDB 3.0: a comprehensive resource for annotation and prediction of
590 animal transcription factors. *Nucleic Acids Res* **47**, gky822 (2018).
591 26.) Macrì, S. *et al.* Hmga2 is required for neural crest cell specification in Xenopus laevis.
592 *Dev Biol* **411**, 25–37 (2016).
593 27.) Kee, Y. & Bronner-Fraser, M. Id4 expression and its relationship to other Id genes during
594 avian embryonic development. *Mech Develop* **109**, 341–345 (2001).
595 28.) Hu, J. *et al.* Endothelin signaling activates Mef2c expression in the neural crest through a
596 MEF2C-dependent positive-feedback transcriptional pathway. *Development* **142**, 2775–
597 2780 (2015).
598 29.) López, S. H. *et al.* Loss of Tbx3 in murine neural crest reduces enteric glia and causes
599 cleft palate, but does not influence heart development or bowel transit. *Dev Biol* **444**,
600 S337–S351 (2018).
601 30.) Seberg, H. E., Otterloo, E. V. & Cornell, R. A. Beyond MITF: Multiple transcription factors
602 directly regulate the cellular phenotype in melanocytes and melanoma. *Pigm Cell*
603 *Melanoma R* **30**, 454–466 (2017).
604 31.) Agarwal, P. *et al.* The MADS box transcription factor MEF2C regulates melanocyte
605 development and is a direct transcriptional target and partner of SOX10. *Development*
606 **138**, 2555–2565 (2011).
607 32.) DiVito, K. A., Trabosh, V. A., Chen, Y., Simbulan-Rosenthal, C. M. & Rosenthal, D. S.
608 Inhibitor of differentiation-4 (Id4) stimulates pigmentation in melanoma leading to
609 histiocyte infiltration. *Exp Dermatol* **24**, 101–107 (2015).
610 33.) Chhabra, Y. *et al.* Genetic variation in IRF4 expression modulates growth characteristics,
611 tyrosinase expression and interferon-gamma response in melanocytic cells. *Pigm Cell*
612 *Melanoma R* **31**, 51–63 (2018).

613 34.) Wang, C. *et al.* Donkey genomes provide new insights into domestication and selection
614 for coat color. *Nat Commun* **11**, 6014 (2020).
615 35.) Imsland, F. *et al.* Regulatory mutations in TBX3 disrupt asymmetric hair pigmentation that
616 underlies Dun camouflage color in horses. *Nat Genet* **48**, 152–158 (2016).
617 36.) Yin, K., Sturm, R. A. & Smith, A. G. MC1R and NR4A receptors in cellular stress and
618 DNA repair: implications for UVR protection. *Exp Dermatol* **23**, 449–452 (2014).
619 37.) Moon, H. *et al.* Melanocyte Stem Cell Activation and Translocation Initiate Cutaneous
620 Melanoma in Response to UV Exposure. *Cell Stem Cell* **21**, 665-678.e6 (2017).
621 38.) Zhang, T. *et al.* Cell-type–specific eQTL of primary melanocytes facilitates identification
622 of melanoma susceptibility genes. *Genome Res* **28**, 1621–1635 (2018).
623 39.) Perotti, V. *et al.* NFATc2 is an intrinsic regulator of melanoma dedifferentiation.
624 *Oncogene* **35**, 2862–2872 (2016).
625 40.) Smith, A. G., Lim, W., Pearen, M., Muscat, G. E. O. & Sturm, R. A. Regulation of NR4A
626 nuclear receptor expression by oncogenic BRAF in melanoma cells. *Pigm Cell Melanoma*
627 *R* **24**, 551–563 (2011).
628 41.) Boyd, S. C. *et al.* Oncogenic B-RAFV600E Signaling Induces the T-Box3 Transcriptional
629 Repressor to Repress E-Cadherin and Enhance Melanoma Cell Invasion. *J Invest*
630 *Dermatol* **133**, 1269–1277 (2013).
631 42.) Lu, J., Li, X.-P., Dong, Q., Kung, H. & He, M.-L. TBX2 and TBX3: The special value for
632 anticancer drug targets. *Biochimica Et Biophysica Acta Bba - Rev Cancer* **1806**, 268–274
633 (2010).
634 43.) Peres, J. *et al.* TBX3 promotes melanoma migration by transcriptional activation of ID1
635 which prevents activation of E-cadherin by MITF. *J Invest Dermatol* (2021)
636 doi:10.1016/j.jid.2021.02.740.
637 44.) Rodriguez, M., Aladowicz, E., Lanfrancone, L. & Goding, C. R. Tbx3 Represses E-
638 Cadherin Expression and Enhances Melanoma Invasiveness. *Cancer Res* **68**, 7872–
639 7881 (2008).

640 45.) Peres, J. *et al.* The Highly Homologous T-Box Transcription Factors, TBX2 and TBX3,
641 Have Distinct Roles in the Oncogenic Process. *Genes Cancer* **1**, 272–282 (2010).
642 46.) Perrot, C. Y. *et al.* GLI2 cooperates with ZEB1 for transcriptional repression of CDH1
643 expression in human melanoma cells. *Pigm Cell Melanoma R* **26**, 861–873 (2013).
644 47.) Heppt, M. V. *et al.* MSX1-Induced Neural Crest-Like Reprogramming Promotes
645 Melanoma Progression. *J Invest Dermatol* **138**, 141–149 (2018).
646 48.) Chen, Y. *et al.* ZEB1 Regulates Multiple Oncogenic Components Involved in Uveal
647 Melanoma Progression. *Sci Rep-uk* **7**, 45 (2017).
648 49.) Goding, C. R. & Arnheiter, H. MITF—the first 25 years. *Gene Dev* **33**, 983–1007 (2019).
649 50.) Murakami, M., Matsuzaki, F. & Funaba, M. Regulation of melanin synthesis by the TGF-β
650 family in B16 melanoma cells. *Mol Biol Rep* **36**, 1247–1250 (2009).
651 51.) Li, J., Weinberg, M. S., Zerbini, L. & Prince, S. The oncogenic TBX3 is a downstream
652 target and mediator of the TGF-β1 signaling pathway. *Mol Biol Cell* **24**, 3569–3576
653 (2013).
654 52.) Laurette, P. *et al.* Transcription factor MITF and remodeller BRG1 define chromatin
655 organisation at regulatory elements in melanoma cells. *Elife* **4**, e06857 (2015).
656 53.) Louphrasitthiphol, P. *et al.* Tuning Transcription Factor Availability through Acetylation-
657 Mediated Genomic Redistribution. *Mol Cell* **79**, 472-487.e10 (2020).
658 54.) Lu, S. *et al.* TBX2 controls a proproliferative gene expression program in melanoma.
659 *Gene Dev* **35**, 1657–1677 (2021).
660 55.) McLean, C. Y. *et al.* GREAT improves functional interpretation of cis-regulatory regions.
661 *Nat Biotechnol* **28**, 495–501 (2010).
662 56.) Strub, T. *et al.* Essential role of microphthalmia transcription factor for DNA replication,
663 mitosis and genomic stability in melanoma. *Oncogene* **30**, 2319–2332 (2011).
664 57.) Praetorius, C. *et al.* A Polymorphism in IRF4 Affects Human Pigmentation through a
665 Tyrosinase-Dependent MITF/TFAP2A Pathway. *Cell* **155**, 1022–1033 (2013).

666 58.) Aoki, H. & Moro, O. Involvement of microphthalmia-associated transcription factor (MITF)
667 in expression of human melanocortin-1 receptor (MC1R). *Life Sci* **71**, 2171–2179 (2002).
668 59.) Visser, M., Kayser, M. & Palstra, R.-J. HERC2 rs12913832 modulates human
669 pigmentation by attenuating chromatin-loop formation between a long-range enhancer
670 and the OCA2 promoter. *Genome Res* **22**, 446–455 (2012).
671 60.) Gautron, A. *et al.* Human TYRP1: two functions for a single gene? *Pigm Cell Melanoma*
672 *R* (2020) doi:10.1111/pcmr.12951.
673 61.) Washkowitz, A. J., Gavrilov, S., Begum, S. & Papaioannou, V. E. Diverse functional
674 networks of Tbx3 in development and disease. *Wiley Interdiscip Rev Syst Biology*
675 *Medicine* **4**, 273–283 (2012).
676 62.) Khan, S. F. *et al*. *Gene* **726**, 144223 (2019).
677 63.) Pape, E. L., Wakamatsu, K., Ito, S., Wolber, R. & Hearing, V. J. Regulation of
678 eumelanin/pheomelanin synthesis and visible pigmentation in melanocytes by ligands of
679 the melanocortin 1 receptor. *Pigm Cell Melanoma R* **21**, 477–486 (2008).
680 64.) Ni, J. *et al.* The effect of the NMDA receptor-dependent signaling pathway on cell
681 morphology and melanosome transfer in melanocytes. *J Dermatol Sci* **84**, 296–304
682 (2016).
683 65.) Tagore, M. *et al.* Electrical activity between skin cells regulates melanoma initiation.
684 *Biorxiv* 2021.12.19.473393 (2021) doi:10.1101/2021.12.19.473393.
685 66.) Enkhtaivan, E. & Lee, C. H. Role of Amine Neurotransmitters and Their Receptors in Skin
686 Pigmentation: Therapeutic Implication. *Int J Mol Sci* **22**, 8071 (2021).
687 67.) Palumbo, A. Melanogenesis in the Ink Gland of Sepia officinalis. *Pigm Cell Res* **16**, 517–
688 522 (2003).
689 68.) Eddy, K. & Chen, S. Glutamatergic Signaling a Therapeutic Vulnerability in Melanoma.
690 *Cancers* **13**, 3874 (2021).
691 69.) Janes, P. W. *et al.* EphA3 biology and cancer. *Growth Factors* **32**, 176–189 (2014).

692 70.) Theveneau, E. & Mayor, R. Neural crest migration: interplay between chemorepellents,
693 chemoattractants, contact inhibition, epithelial–mesenchymal transition, and collective
694 cell migration. *Wiley Interdiscip Rev Dev Biology* **1**, 435–445 (2012).
695 71.) Pape, E. L. *et al.* Microarray analysis sheds light on the dedifferentiating role of agouti
696 signal protein in murine melanocytes via the Mc1r. *Proc National Acad Sci* **106**, 1802–
697 1807 (2009).
698 72.) Arnheiter, H. The discovery of the microphthalmia locus and its gene, Mitf. *Pigm Cell*
699 *Melanoma R* **23**, 729–735 (2010).
700 73.) Levy, C., Khaled, M. & Fisher, D. E. MITF: master regulator of melanocyte development
701 and melanoma oncogene. *Trends Mol Med* **12**, 406–414 (2006).
702 74.) Li, J. *et al.* The Anti-proliferative Function of the TGF-β1 Signaling Pathway Involves the
703 Repression of the Oncogenic TBX2 by Its Homologue TBX3*. *J Biol Chem* **289**, 35633–
704 35643 (2014).
705 75.) Mesbah, K. *et al.* Identification of a Tbx1/Tbx2/Tbx3 genetic pathway governing
706 pharyngeal and arterial pole morphogenesis. *Hum Mol Genet* **21**, 1217–1229 (2012).
707 76.) Mohan, R. A. *et al.* T-box transcription factor 3 governs a transcriptional program for the
708 function of the mouse atrioventricular conduction system. *Proc National Acad Sci* **117**,
709 18617–18626 (2020).
710 77.) Singh, R. *et al.* Tbx2 and Tbx3 induce atrioventricular myocardial development and
711 endocardial cushion formation. *Cell Mol Life Sci* **69**, 1377–1389 (2012).
712 78.) Lüdtke, T. H. *et al.* Tbx2 and Tbx3 Act Downstream of Shh to Maintain Canonical Wnt
713 Signaling during Branching Morphogenesis of the Murine Lung. *Dev Cell* **39**, 239–253
714 (2016).
715 79.) Sheeba, C. J. & Logan, M. P. O. Chapter Twelve The Roles of T-Box Genes in
716 Vertebrate Limb Development. *Curr Top Dev Biol* **122**, 355–381 (2017).

717 80.) Frank, D. U., Emechebe, U., Thomas, K. R. & Moon, A. M. Mouse Tbx3 Mutants Suggest
718 Novel Molecular Mechanisms for Ulnar-Mammary Syndrome. *Plos One* **8**, e67841
719 (2013).
720 81.) Kaiser, M. *et al.* Regulation of otocyst patterning by Tbx2 and Tbx3 is required for inner
721 ear morphogenesis in the mouse. *Development* **148**, dev.195651 (2021).
722 82.) Dong, L. *et al.* Novel HDAC5-interacting motifs of Tbx3 are essential for the suppression
723 of E-cadherin expression and for the promotion of metastasis in hepatocellular
724 carcinoma. *Signal Transduct Target Ther* **3**, 22 (2018).
725 83.) Peres, J. & Prince, S. The T-box transcription factor, TBX3, is sufficient to promote
726 melanoma formation and invasion. *Mol Cancer* **12**, 117 (2013).
727 84.) Hoekstra, H. E. Genetics, development and evolution of adaptive pigmentation in
728 vertebrates. *Heredity* **97**, 222–234 (2006).
729 85.) Chintala, S. *et al.* Slc7a11 gene controls production of pheomelanin pigment and
730 proliferation of cultured cells. *P Natl Acad Sci Usa* **102**, 10964–10969 (2005).
731 86.) Poltorack, C. D. & Dixon, S. J. Understanding the role of cysteine in ferroptosis: progress
732 & paradoxes. *Febs J* **289**, 374–385 (2022).
733 87.) Willmer, T., Peres, J., Mowla, S., Abrahams, A. & Prince, S. The T-Box factor TBX3 is
734 important in S-phase and is regulated by c-Myc and cyclin A-CDK2. *Cell Cycle* **14**, 3173–
735 3183 (2015).
736 88.) Damerell, V. *et al.* The c-Myc/TBX3 Axis Promotes Cellular Transformation of Sarcoma-
737 Initiating Cells. *Frontiers Oncol* **11**, 801691 (2022).
738 89.) Coll, M., Seidman, J. G. & Müller, C. W. Structure of the DNA-Bound T-Box Domain of
739 Human TBX3, a Transcription Factor Responsible for Ulnar-Mammary Syndrome.
740 *Structure* **10**, 343–356 (2002).
741 90.) Langmead, B. & Salzberg, S. L. Fast gapped-read alignment with Bowtie 2. *Nat Methods*
742 **9**, 357–359 (2012).

743 91.) Zhang, Y. *et al.* Model-based Analysis of ChIP-Seq (MACS). *Genome Biol* **9**, R137
744 (2008).
745 92.) Bailey, T. L., Johnson, J., Grant, C. E. & Noble, W. S. The MEME Suite. *Nucleic Acids*
746 *Res* **43**, W39–W49 (2015).
747 93.) Quinlan, A. R. & Hall, I. M. BEDTools: a flexible suite of utilities for comparing genomic
748 features. *Bioinformatics* **26**, 841–842 (2010).
749 94.) Yu, G., Wang, L.-G. & He, Q.-Y. ChIPseeker: an R/Bioconductor package for ChIP peak
750 annotation, comparison and visualization. *Bioinformatics* **31**, 2382–2383 (2015).

Figures and Tables

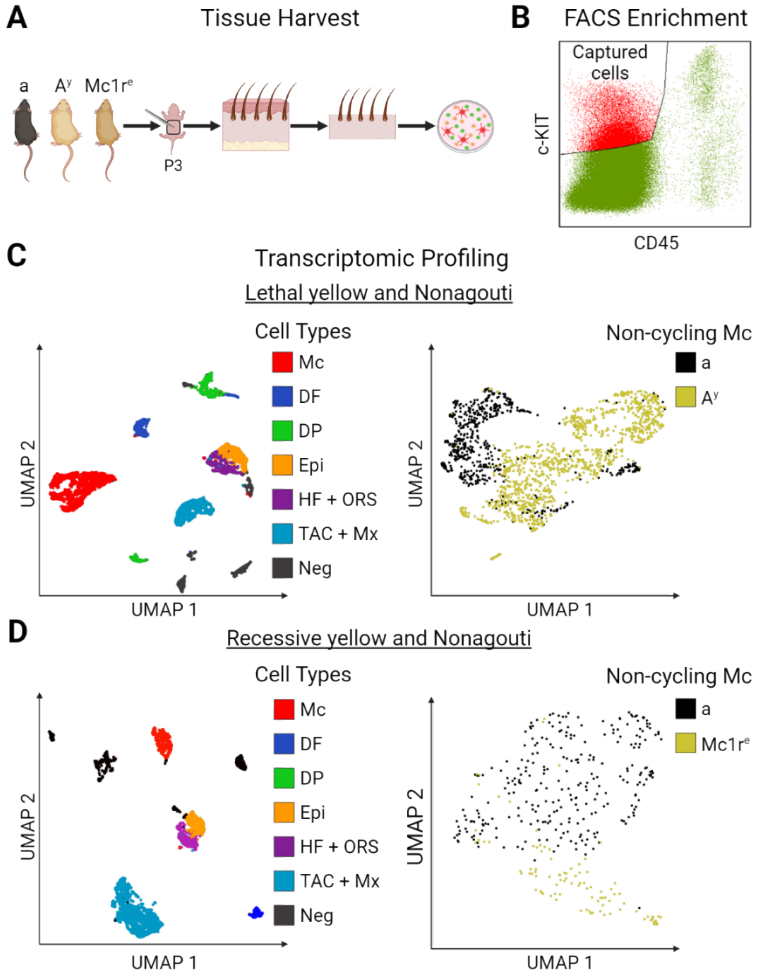

Figure 1. Overview of single cell sequencing of primary murine melanocytes. (A) Schematic of tissue harvest and digestion for melanocyte isolation from dorsal skin (a = nonagouti; A^y = lethal yellow, $Mc1r^e$ = recessive yellow). (B) Representative FACS enrichment of c-KIT^+/$CD45^-$ cells isolated from the lethal yellow sample (red). (C-D) Uniform Manifold Approximation and Projection (UMAP) plots of the sequenced cells that passed quality control for each pairwise experiment. Among the cells isolated from nonagouti and lethal yellow paired samples (6,413 cells in C) and nonagouti and recessive yellow paired samples (4645 cells in D), skin cell types were identified and labeled as follows: Melanocytes (Mc), Dermal fibroblasts (DF), Dermal papilla (DP), Epidermis (Epi), Hair follicle and Outer root sheath (HF + ORS), and Transit amplifying and Matrix cells (TAC + Mx). Right panels show UMAP plots of the 2256 cells classified as non-cycling melanocytes. The

764 nonagouti melanocytes (black) segregate from the recessive yellow and lethal yellow (gold)
765 melanocytes consistent with a eumelanin and pheomelanin producing melanocytes having distinct
766 transcriptional profiles.

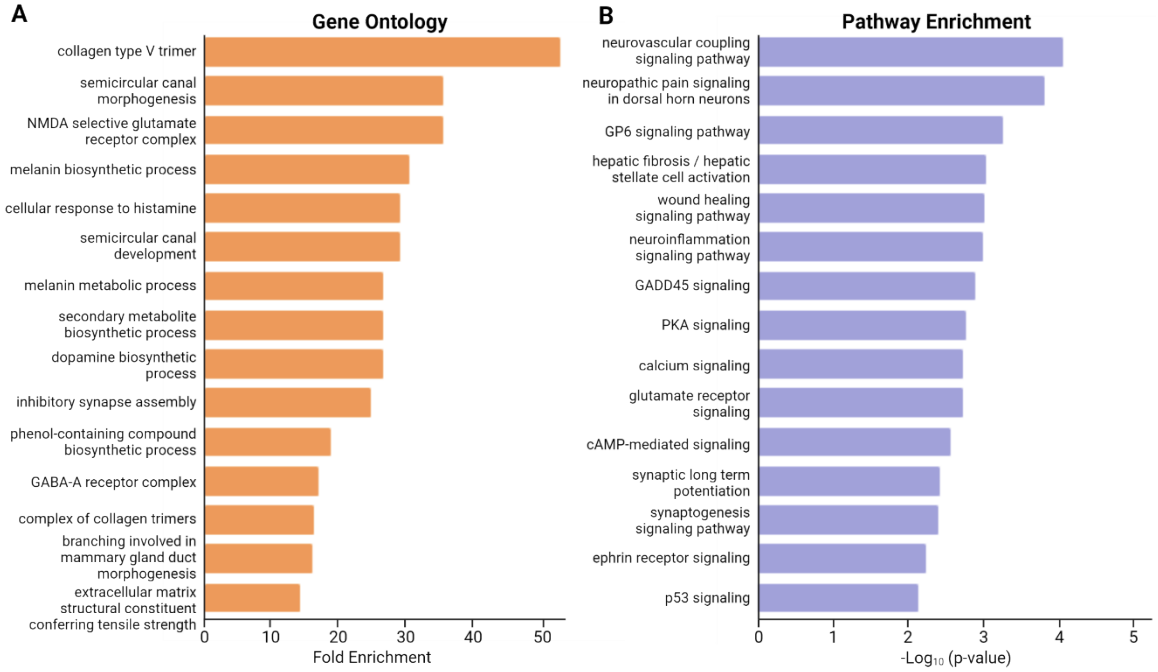

Figure 2. Enriched processes and pathways present in the PGS. (A) Top 15 significant GO terms ranked by fold-enrichment (FDR < 0.05). (B) Top 15 significant pathway terms from IPA ranked by significance (p-value <0.05).

A

	Lethal yellow		Recessive yellow	
TF	FDR step up	Fold change	FDR step up	Fold change
Plagl1	7.02E-74	-4.95	4.49E-16	-7.74
Id4	9.10E-41	4.32	1.12E-06	4.06
Mef2c	8.98E-40	2.69	1.93E-07	2.33
Tfap2b	4.41E-26	2.56	1.73E-05	2.30
Zeb1	1.21E-24	-2.14	9.35E-08	-2.50
Tbx3	6.32E-20	5.62	1.31E-24	16.73
Irf4	1.32E-19	-3.02	7.19E-03	-2.61
Ar	1.02E-17	-3.49	6.09E-05	-11.40
Hmga2	1.34E-12	5.72	2.41E-04	4.11
Zfhx4	4.70E-11	-2.71	4.77E-05	-23.02
Rorb	8.80E-09	-2.17	1.73E-02	-4.24
Pgr	2.68E-08	10.98	2.15E-10	15.85
Prrx2	1.04E-04	2.65	2.71E-03	3.57
Nr4a2	1.06E-03	2.46	1.96E-31	7.30
Prrx1	4.02E-03	3.69	1.76E-02	3.69
Co-TF				
Eya1	2.95E-37	-3.05	2.38E-37	-11.24
Lmo2	3.15E-36	11.61	8.78E-15	6.91
Padi2	2.86E-16	3.27	3.51E-08	4.82
Cbfa2t3	2.43E-16	5.94	1.65E-06	3.72
Pcbd1	1.25E-03	2.12	2.37E-02	2.34
Runx1t1	3.60E-03	4.19	1.19E-09	10.85
Hdac9	4.05E-02	3.47	1.02E-02	7.52

B

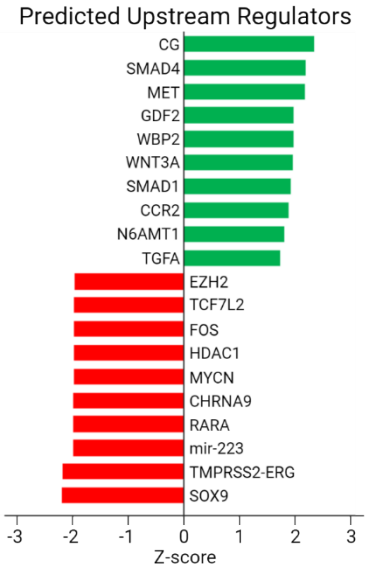

Figure 3. Identifying PGS regulatory factors. (A) List of all differentially expressed transcription/co-transcription factors found within the PGS and ranked by FDR from the nonagouti/lethal yellow pairwise differential analysis. (B) Top 10 predicted activated (green) and inhibited (red) regulators of the PGS gene list ranked by Z-score.

Figure 4. ChIP-seq analysis implicates TBX3 as a regulator of melanogenesis. (A) Position of called TBX3 peaks relative to the TSS. (B) ChIPseeker plot identifying genomic regions in which TBX3 is bound. (C) Top 15 GO terms of genes associated with TBX3 ChIP target genes ranked by $-\text{Log}_{10}$ of the FDR. (D) Top 5 predicted phenotype associations (human and mouse) from TBX3 ChIP gene by $-\text{Log}_{10}$ of the FDR.

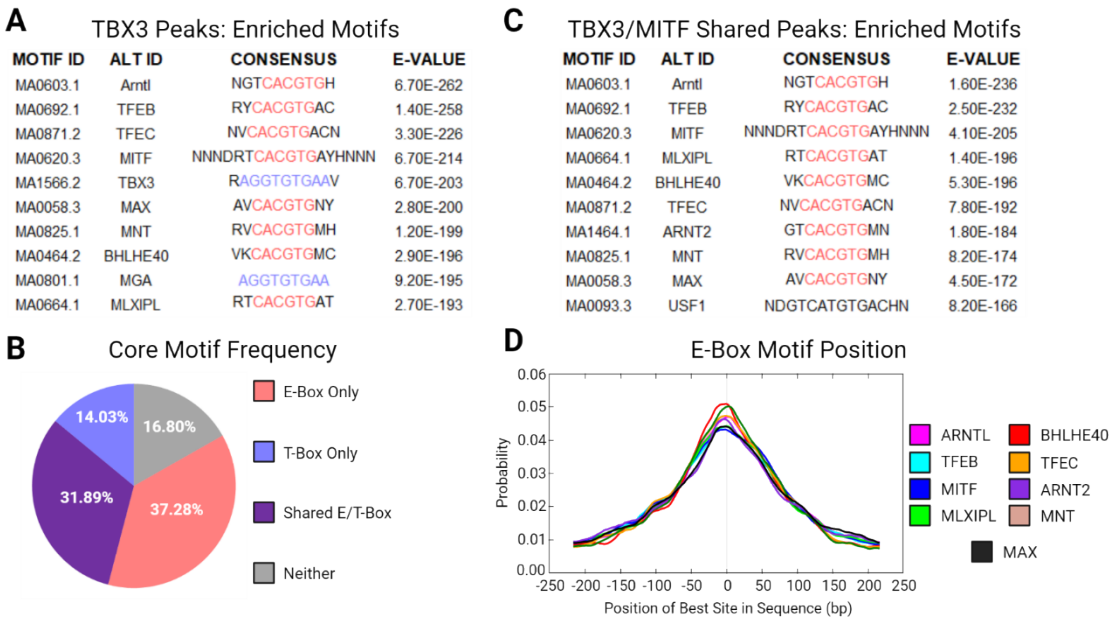

Figure 5. TBX3 binds MITF targets at E-boxes. (A) The top 10 motifs enriched within TBX3 ChIP peaks show over-representation of core E-box (red) and T-box (purple) sequences (B) The majority of TBX3 ChIP peaks contain either a T-box motif (14%), E-box motif (27%), or both (32%). (C) Top motifs of shared MITF and TBX3 peak sites (E-box = red; T-box = purple). (D) CentriMo plot showing top 9 centrally bound motifs.

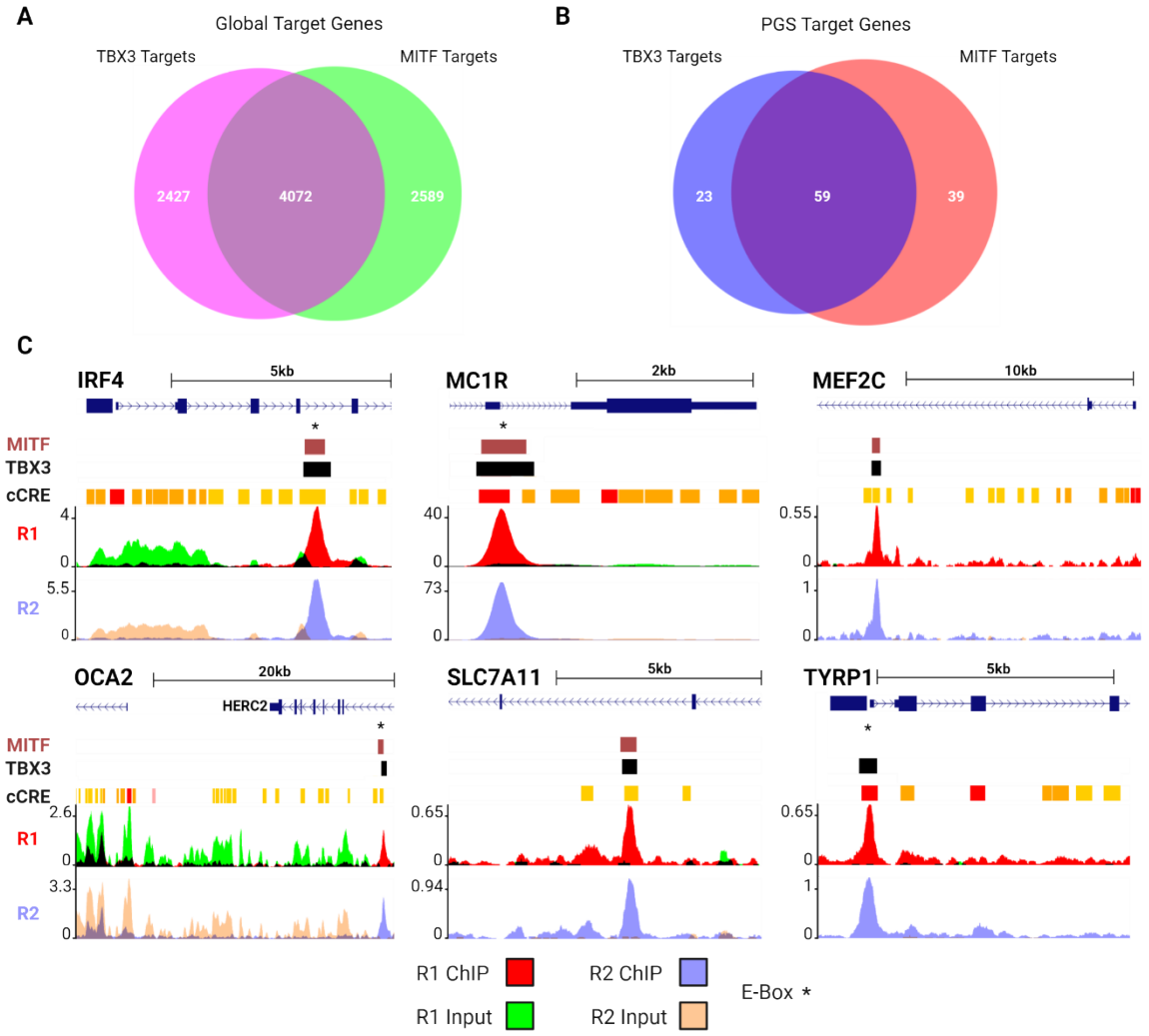

Figure 6. TBX3 binds the E-box of pigmentation gene targets. (A) Intersection showing the number of murine genes (4072) associated with ChIP peaks in both our TBX3 dataset and a published MITF dataset. (B) Intersection of PGS genes identified as targets of both TBX3 and MITF. (C) UCSC browser view of TBX3 and MITF ChIP peaks associated with pigmentation genes. Browser tracks are as follows: TBX3 = replicated binding sites in our dataset; MITF = ChIP peaks from Strub et al; cCRE=encode annotated candidate cis-regulatory elements. The location of verified MITF regulatory elements containing E-box motifs are indicated (*) (refs in text).

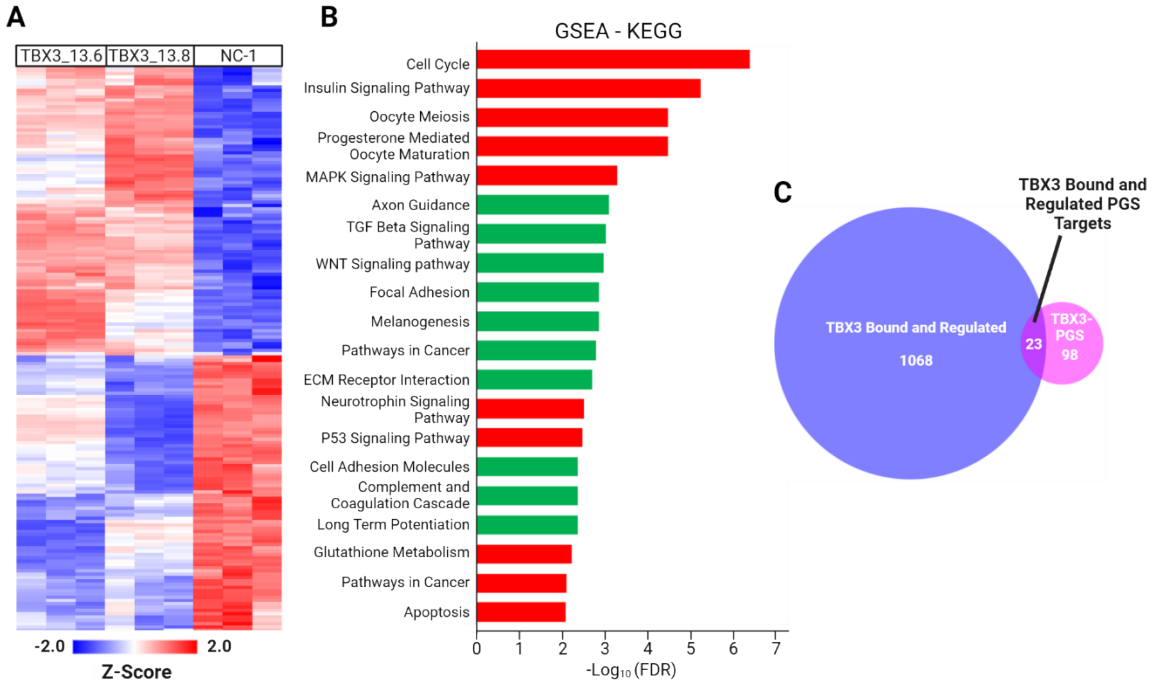

Figure 7. TBX3 binds to and regulates PGS genes. (A) Heatmap depicting relative gene expression of 2780 DEG (Adjusted p-value < 0.05) from the TBX3 knockdown samples against a non-coding control. (B) Top KEGG terms ranked by -Log_{10} of the p-value for upregulated (green) and downregulated (red) genes. (C) Intersection of DE TBX3 gene targets against PGS TBX3 targets.

803 **Table 1. Pigmentation phenotype associated genes found within the Pheomelanin Gene**
804 **Signature (PGS)** with FDR and FC values for each pairwise experiment. In each pairwise
805 experiment a negative FC indicates reduced expression in the pheomelanin producing
806 melanocytes (lethal yellow, recessive yellow) compared to the eumelanin producing melanocytes
807 isolated from nonagouti littermates.
808

	Lethal yellow		**Recessive yellow**	
Gene	FDR step up	Fold change	FDR step up	Fold change
Tyrp1	0.00E+00	-19.31	1.12E-67	-83.90
Pmel	4.82E-46	-2.33	5.82E-16	-2.55
Mef2c	8.98E-40	2.69	1.93E-07	2.33
Oca2	1.77E-25	-3.16	9.28E-05	-2.47
Slc7a11	5.38E-23	7.72	3.79E-03	3.92
Irf4	1.32E-19	-3.02	7.19E-03	-2.61
Mc1r	2.58E-11	2.94	3.64E-03	3.63
Gas7	1.37E-07	-2.28	1.05E-02	-8.57
Sdc2	1.70E-07	2.39	8.94E-13	4.29
Pcbd1	1.25E-03	2.12	2.37E-02	2.34
Masp1	9.76E-03	3.11	1.73E-02	2.69

809
810

811 # Supporting Information

812 **S1 Fig. Classification Scheme for nonagouti and lethal yellow cells.** (A) Uniform Manifold
813 Approximation and Projection (UMAP) plot of lethal yellow and nonagouti cells classified by skin
814 cell type: Melanocytes (Mc), Dermal fibroblasts (DF), Dermal papilla (DP), Epidermis (Epi), Hair
815 follicle and Outer root sheath (HF + ORS), and Transit amplifying and Matrix cells (TAC + Mx). (B)
816 UMAP of cells classified by graph-based cluster. (C) UMAPs depicting heatmap of cell type scoring.
817

818 **S2 Fig. Classification Scheme for nonagouti and recessive yellow cells.** (A) Uniform Manifold
819 Approximation and Projection (UMAP) plot of the recessive yellow and nonagouti cells classified
820 by skin cell type: Melanocytes (Mc), Dermal fibroblasts (DF), Dermal papilla (DP), Epidermis (Epi),
821 Hair follicle and Outer root sheath (HF + ORS), and Transit amplifying and Matrix cells (TAC + Mx).
822 (B) UMAP of cells classified by graph-based cluster. (C) UMAPs depicting heatmap of cell type
823 scoring.
824

825 **S3 Fig. Melanocytes cell cycle.** (A) Total melanocytes from lethal yellow and nonagouti pairwise
826 experiment (left), cells within the cell cycle highlighted in blue (right). (B) Total melanocytes from
827 recessive yellow and nonagouti pairwise experiment (left), cells within the cell cycle highlighted in
828 blue (right).
829

830 **S4 Fig. Inducible TBX3 cell line validation.** (A) schematic of piggyBAC transposase system with
831 Tet-on inducible expression of TBX3. Dox, doxycycline; TRE, tetracycline response element; rtTA,
832 reverse tetracycline-controlled transactivator. (B) Western blot of polyclonal 501mel-iTBX3-3xHA-
833 PuroR inducible cells treated with varying amounts of doxycycline for 24h. (C) Venn diagram
834 depicting shared peaks between both replicate ChIP experiments. (D) UCSC browser view of TBX3
835 and MITF ChIP peaks associated with E-cadherin. Browser tracks are as follows: TBX3 = replicated

836 binding sites in our dataset; MITF = ChIP peaks from Strub et al; cCRE=encode annotated
837 candidate cis-regulatory elements.
838
839 **S5 Fig. Motif enrichment by fold-change direction in TBX3 KD studies.** (A) Top 10 motifs,
840 ranked by e-value, of TBX3 ChIP peaks associated with putative target genes with increased
841 expression (left) or decreased expression (right) upon TBX3 knock-down.
842
843 **S1-S5 Figure File. Berns et al_Supplementary Figures S1-S5.doc.**
844
845 **S1 Table. Gene Signature of Murine Skin Cells from Rezza et al.**
846
847 **S2 Table. Pheomelanin Gene Signature.**
848
849 **S3 Table. GREAT Output for TBX3 ChIP Dataset.**
850
851 **S4 Table. GREAT Output for MITF ChIP Dataset.**
852
853 **S5 Table. Human to Mouse Conversion of TBX3 Target Genes.**
854
855 **S6 Table. Human to Mouse Conversion of MITF Target Genes.**
856
857 **S7 Table. Gene Target Overlap.**
858
859 **S8 Table. Significant Differentially Expressed Genes from TBX3 Knockdown.**
860
861 **S9 Table. Significant Differentially Expressed Genes from TBX3 Knockdown which are TBX3**
862 **Targets Identified by ChIP.**

863

864 **S1-S9 Tables File. Berns et al_Supplementary Tables S1-S9.xls.**